JNCS
Journal of Nepal Chemical Society
March/April 2023, Vol. 43, No. 2, 70-90
ISSN: 2091-0304 (print)
DOI: https://doi.org/10.3126/jncs.v43i2.53343
RESEARCH ARTICLE

Chemical Synthesis, Characterization, and Computational Investigation of Two Schiff Bases Derived From 3-(2-Hydroxyphenyl)-4-Amino-4H-1,2,4-Triazole-5-Thiol and their Corresponding Oxovanadium(IV) Complexes

Bharat Prasad Sharma[1], Jhashanath Adhikari Subin[2,*], Khim Prasad Panthi[3], Sarvesh Kumar Pandey[4], Akeel Ahamd[5], Akhilesh Kumar Srivastava[4], Motee Lal Sharma[1,*]

[1]Central Department of Chemistry, Tribhuvan University, Kirtipur, Kathmandu 44618, Nepal

[2]Bioinformatics and Cheminformatics Division, Scientific Research and Training Nepal P. Ltd., Madhyapur Thimi-3, Bhaktapur 44800, Nepal

[3]Department of Chemistry, Tri-Chandra Multiple Campus, Tribhuvan University, Kathmandu 44613, Nepal

[4]Department of Chemistry, DDU Gorakhpur University, Gorakhpur, Uttar Pradesh 273009, India

[5]Department of Chemistry, Mirza Ghalib College, Gaya, Bihar 82300, India

*Corresponding authors: ml.sharma@cdc.tu.edu.np(M. L. Sharma),subinadhikari2018@gmail.com (J. Adhikari Subin)

Submitted: 16 Dec 2022, Revised: 7 Feb 2023, Accepted: 12 Feb 2023

Abstract

A triazole, 2-(4-amino-5-mercapto-4H-1,2,4-triazol-3-yl)phenol, has been prepared from *2*-hydroxybenzoic acid by routine multi-step chemical synthesis. It was then used in synthesizing two different Schiff base ligands (L_1 and L_2). Their respective oxovanadium(IV) complexes (ML_1 and ML_2) were consequently synthesized and characterized by different experimental techniques like elemental analysis, FTIR spectroscopy, UV-Visible spectroscopy, and EPR spectrometry. The cyclic voltammetry measurements showed electrochemically stable nature of the complexes. The powder X-ray diffraction patterns revealed the presence of monoclinic crystals with particle sizes of *ca*. 15-17 nm for both the complexes. DFT calculations were performed for the determination of geometrical models, energetic stability, electronic properties, spectral features, and reactivity of the synthesized ligands and the complexes. The spectral characterization of the complexes suggests a square-pyramidal geometry around VO(IV) and was supported by computational results derived from the proposed models. This work shows that computational calculation along with experimental characterization provides better insights into new chemical compounds and their properties that could be performed in parallel as a regular tool.

Keywords: *Synthesis, Triazole, Oxovanadium(IV) complexes, Schiff bases, DFT calculation*

1. Introduction

Oxovanadium(IV) complexes are a class of organo-metallic compounds that have characteristic structure where an oxygen atom is bonded to vanadium atom by a double bond at the apical position of the molecule. Due to prominent efficacy of this group towards screening against different disease-causing agents, the coordination complexes containing this moiety has garnered augmented interest in the field of biological chemistry and medicinal chemistry [1]. Although many other medicinal properties of vanadium complexes like the insulin mimetic property have been studied extensively in the past decades, its complexes with Schiff bases were not able to underscore their effectiveness in the treatment of other different types of diseases. But the recent discovery of several VO(IV) complexes with various classes of Schiff bases having distinct therapeutic potentials against multitude of illness have revived

its global attraction in pharmacology [2, 3]. In recent years, important metal chelators, Schiff bases and their numerous forms, are being discovered for the treatment of diseases like bacterial, fungal, and viral infections, tuberculosis, tumor, etc. [4, 5]. The study of chemistry and biological performances of the vanadium complexes with different chelators and complexation agents by changing their substituting functional groups have added novelty to this type of research.

Due to synergistic advantages with experimental methods, computational modeling has emerged as a quick and viable support in the characterization of compounds. It helps in calculating and analyzing the electronic and structural properties, transport and optical properties, interactions and types of bonding, and other distinct features for specialized applications [3, 6]. The computational approach helps to acquire a thorough understanding of the correlation between the structure of the studied compounds and its properties by revealing the structural and spectroscopic features at the atomic level, the reaction mechanisms, electronic rearrangement, and minimum energy conformers [7, 8].

Due to the rapid increment in the importance of both Schiff bases and oxovanadium moiety in the vanadium complexes, new compounds were synthesized and characterized by different experimental methods. Their structural and electronic features were evaluated by DFT calculation based on different models for complementary support and justification of the outcomes.

2. Materials and Methods

2.1 Synthesis of Schiff bases

2-Hydroxy benzoate was synthesized from the esterification of 0.1 mole of 2-hydroxy benzoic acid by refluxing it with methanol in presence of conc. H_2SO_4 at 50 °C for about 5 h and then, it was isolated by pouring it into ice water using a separating funnel. The synthesized ester was allowed to reflux with hydrazine hydrate at 45 °C for about 4 h. Then the reaction mixture was reduced to half its volume and cooled whereby white elongated crystals of hydrazide were obtained.

1 mole of hydrazide was dissolved in 1 mole of alc. KOH solution and allowed to react with of 1.1 moles of CS_2 (added dropwise) at ice cold temperature with constant stirring for 5-6 h. Then cream-colored thick liquid was obtained from which white solid was separated and allowed to reflux with an excess of hydrazine hydrate (~ 1.5 moles) for about 5 h at 45 °C. Amino-mercapto-triazole prepared was separated, recrystallized and dried[9, 10].

The Schiff bases (L_1 and L_2) were synthesized by refluxing 0.1 mole of triazole with 0.1 mole of benzaldehyde and 0.1 mole of acetophenone respectively in ethanol at 50 °C for about 7 h. When the color of the reaction mixture turned brown, it was concentrated to half its volume and allowed to cool overnight [L_1–L_2]. The brown crystals of ligand L_1 and L_2 were obtained by recrystallization in 10% ethanol.

2.2 Synthesis of oxovanadium(IV) complexes

A mixture of 0.1 mole of vanadyl sulfate with 0.2 mole of respective Schiff base ligand L_1 and L_2 was taken with ethanol solvent and resulting solutions were refluxed at 50 °C for about 8 h to synthesize new oxovanadium(IV) complexes, ML_1 and ML_2 respectively [14, 15]. The tiny crystals of oxovanadium(IV) complexes were grown in mother liquor in cold environment (recrystallization for few days) which resulted in the formation of light green colored crystals.

2.3 Characterization

The solubility tests, melting point determination, and purity tests by the TLC method were performed to characterize the physical properties of synthesized Schiff base ligands and their corresponding oxovanadium(IV) complexes. The XRD patterns were recorded in a D2 phase diffractometer (Bruker, Germany), with 2θ value from 10 to 80 degrees using a Cu-Kα (λ=1.54056 Å) source. The electronic spectra were recorded using a double beam spectrophotometer of Plantronics Model LT-2802 in

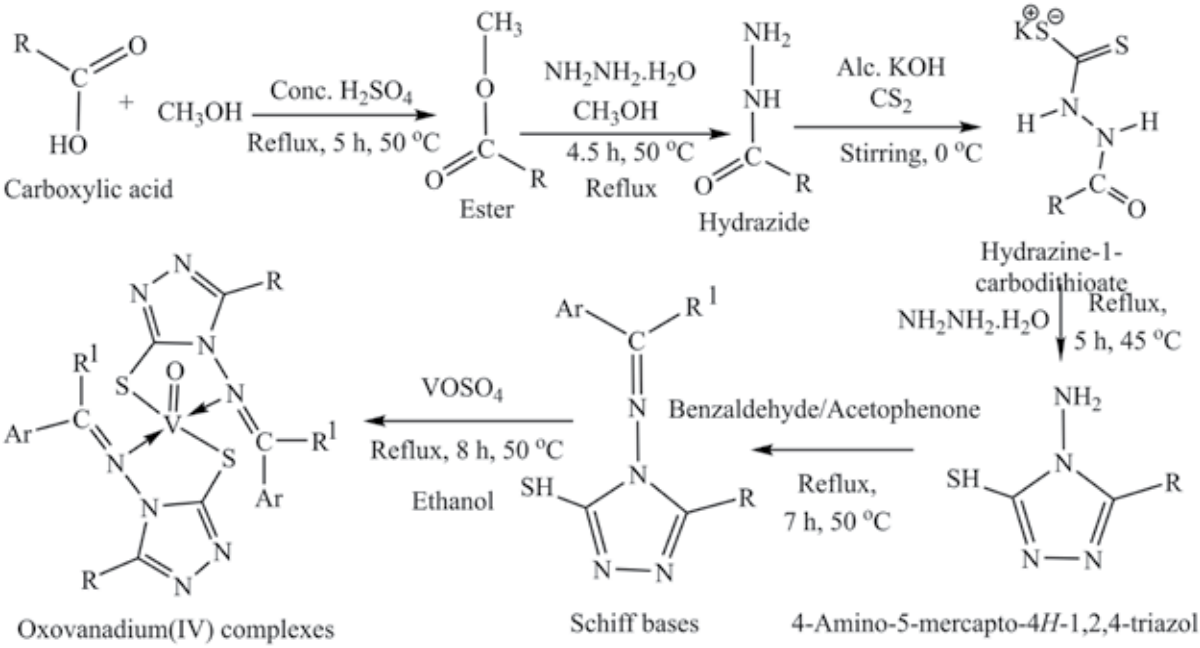

***Scheme 1**: Synthetic route for the Schiff bases and their oxovanadium(IV) complexes [where, R = 2-hydroxybenzyl group and R^1 = H,(for L_1 and ML_1) and CH_3 (for L_2 and ML_2)].*

the range of 250–800 nm in DMSO. FTIR spectra were recorded on the IR Tracer-100 (SHIMADZU, Japan), within the spectral range 4000–400 cm^{-1}. The molar conductance of the samples was measured on the Delux Conductivity Meter of model-601 (India). The EPR spectra for oxovanadium(IV) complexes were obtained at room temperature at field set 3200 G (= 0.32 T), microwave power 5 mW, and microwave frequency 9.1 GHz. The cyclic voltammetry (CV) experiments were conducted on Hokutodenko Galvanostat, model no. 151 (Japan), by using two graphite electrodes as the working electrode and supporting/counter electrode and a standard calomel electrode (SCE) as a reference electrode in 1 mM sample solution with tetrabutylammonium bromide (TBAB) as a supporting electrolyte [16].

2.4 DFT calculation

The synthesized Schiff bases (L1 and L2) and their oxovanadium(IV) complexes (ML1 and ML2) were subjected to DFT study using CP2K program package [17]. The reaction energies, optimized geometries, frontier molecular orbitals (FMOs), and atomic charges were calculated by employing hybrid density functional BLYP, molecular optimized basis set DZVP-MOLOPT-SR-GTH and GTH-BLYP potential at the molecular level in gas phase [3, 18]. The geometry optimization of synthesized compounds was done through a sequential process by initiating from a guess structure with non-stringent convergence criteria and continuing from the converged geometry with strict criteria (lower energy and force with small step sizes) as the structures moved towards the local minima. The final structure at the global minima of the complex potential energy surface (PES) was again distorted to check for the convergence of the optimization process. The similar results from multiple input geometries suggested the attainment of same global minima and was subjected to further characterization and analysis.

The input files for the computational simulation were created by considering the molecule inside a box of size (25 x 25 x 25) au3 where the topology was set to center for non-periodic calculations. The spin multiplicity of vanadium (L=2) and van der Waals dispersion interactions using the DFT-D3 method were also implemented [3]. Gaussian and Augmented Plane Wave (GAPW) method and a non-periodic MT solver were used with the number of grid point equal to 5, a kinetic energy cutoff of 500 au, and a relative cutoff of 100 au. With these parameters, the self-consistent cycles (SCF) converged smoothly, and were considered well suited for similar type of

Table 1: *Physical properties and elemental analysis data of ligands and their complexes*

	Molecular Formula	M.W.	M. P.(°C)	% Experimental Elemental Composition (Theoretical)					
				C	H	N	S	O	V
L_1	$C_{15}H_{12}N_4OS$ (Light brown)	296	174	60.79 (60.80)	4.09 (4.08)	18.89 (18.91)	10.80 (10.82)	5.42 (5.40)	-
L_2	$C_{16}H_{14}N_4OS$ (Light brown)	310	167	61.93 (61.92)	4.57 (4.55)	18.04 (18.05)	10.32 (10.33)	5.14 (5.15)	-
ML_1	$C_{30}H_{22}N_8O_3S_2V$ (Dark green)	657	233	54.78 (54.79)	3.39 (3.37)	17.01 (17.04)	17.05 (17.04)	7.32 (7.30)	7.74 (7.75)
ML_2	$C_{32}H_{26}N_8O_3S_2V$ (Dark green)	685	219	56.04 (56.05)	3.83 (3.82)	16.33 (16.34)	9.33 (9.35)	7.02 (7.00)	7.43 (7.43)

calculations. Broyden type of mixing (*alpha* 0.2) and *nbroyden* 5, *restart* option for successive calculations, and diagonalization with standard algorithm were considered appropriate for the simulation. The convergence criteria (final structures) in terms of energy and force were set to 1.0×10^{-6} Hartree and 5.0×10^{-4} Hartree/Bohr respectively [19, 20].

The EPR *g*-value of the optimized structures of both the oxovanadium(IV) complexes were calculated using an open-source computational chemistry package, NWChem 7.0.0 [21] with 6-31G* basis set, BLYP functional, relativistic zora, and grid settings of medium by adapting cutoff equals to 1.0×10^{-30} Ry, zora cutoff for NMR of 1×10^{-8} Ry, multiplicity equal to 2, maximum iterations of 300, convergence energy of 1×10^{-8}Ry, and property directive with *g* shift option [22]. Higher basis sets required very large memory and computational processing power and were not performed. The optimized geometries of molecules were visualized using Avogadro program [23], and 3D FMOs plots were pictured and analyzed with the help of VESTA program [24].

3. Results and Discussions

3.1 Synthesis and characterization

The synthesized ligands and complexes were colored crystalline solids having high melting point and were soluble in DMSO, acetonitrile, and dimethyl formamide (DMF). The purity tests (TLC method) for all the recrystallized samples using 30% ethyl acetate in hexane showed a single spot indicating the presence of a single component. The yield of the triazole product was 47-63% and that of two ligands were 57-69% and 61-72% respectively. The synthesis of oxovanadium(IV) complexes was repeated three times and the yield was 53-67% for ML_1 and 57-63% for ML_2. The elemental data of the synthesized ligands and complexes validated the purity of the investigated samples within the experimental error. The physicochemical properties like melting point (M.P.), molecular weight (M.W.), color, and the composition of the ligands and their complexes are listed in **Table 1**.

3.2 Spectral characterization

3.2.1 Vibrational spectra

The FTIR spectral analysis of the ligands and the complexes were performed to investigate the functional group and bonding sites present in the compounds. The IR spectra of the ligands and complexes are portrayed in **Fig. 1** and **Fig. 2**. The ligands are characterized by the presence of major functional groups like imine C=N group, triazole C=N group, C=S group, S-H group, O-H group, and 2° N-H group. The absence of bands due to the carbonyl group and primary amine group also validates the formation of the imine group in the complexes. The presence of the V-N band, V-S band, and absence of S-H band and C=S bands in the complexes validate the structural conformation of the final products [3]. The different vibrational bands present in the ligands and complexes are summarized in **Table 2**.

The FT-IR spectra of the ligands, L_1 and L_2 showed a strong stretching band at 1654 cm^{-1} and 1658 cm^{-1} respectively, due to the ν(C=N) imine group but this band shifted to a lower frequency in the spectra of both

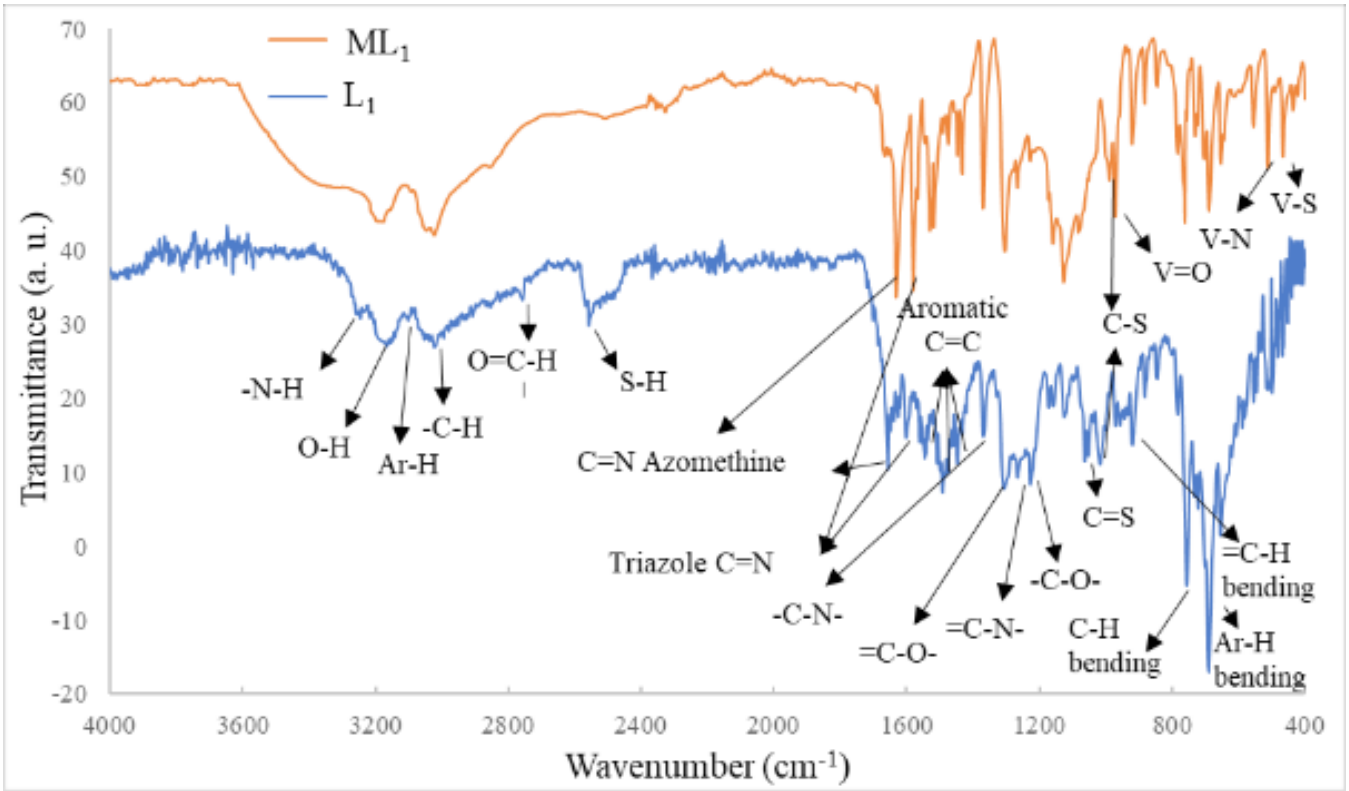

Fig.1: *FTIR spectra oftheligand L_1 and itsoxovanadium(IV)complexML_1.*

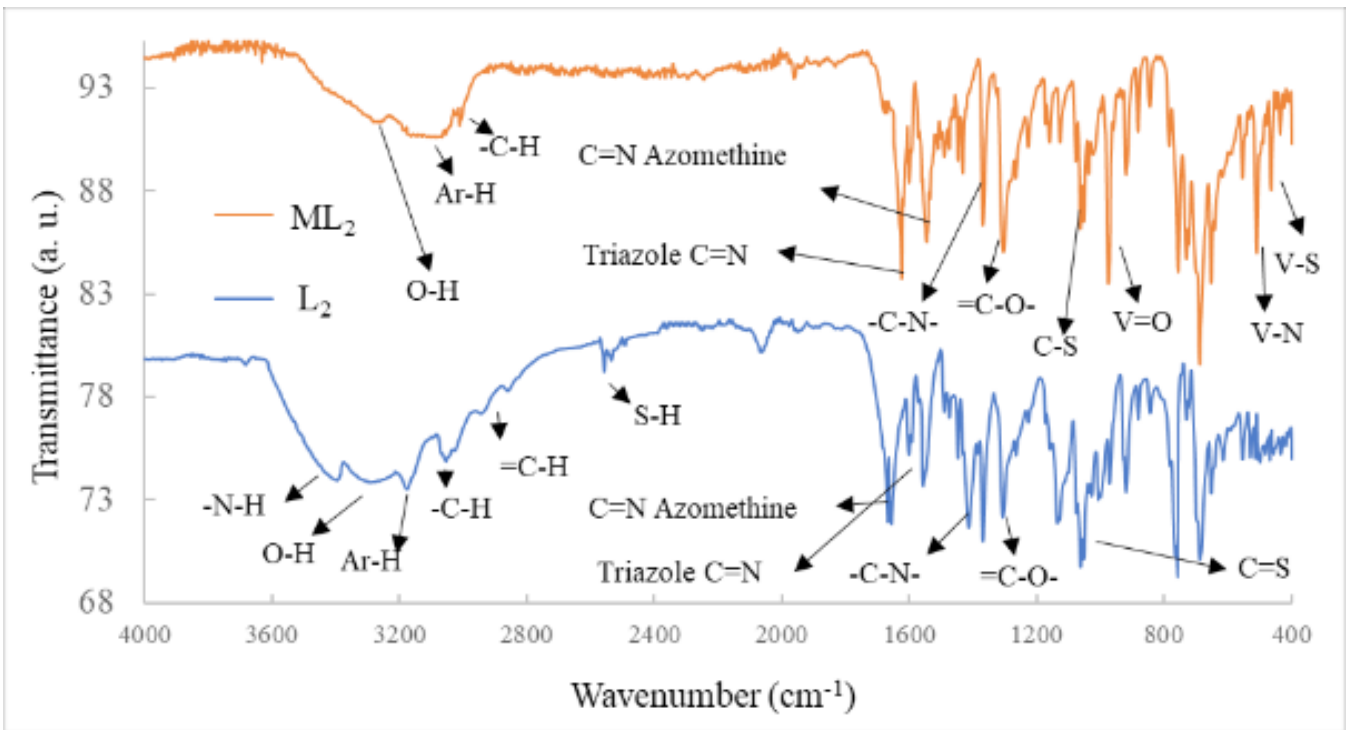

Fig.2: *FTIR spectra oftheligand L_2 and itsoxovanadium(IV)complexML_2.*

Table 2: *Characteristic FT-IR bands (4000–400 cm^{-1}) for different functional groups present in the Schiff base ligands and their oxovanadium(IV) complexes*

Functional Groups	Wavenumber (cm^{-1}) of Bands			
	L_1	L_2	ML_1	ML_2
Azomethine C=N	1654	1658	1627	1624
Triazole C=N	1597	1544	1586	1543
-C-N-	1366	1365	1367	1369
=C-N-	1263	1265	1265	1266
-C-O-	1226	1227	1224	1226
=C-O-	1305	1304	1301	1303
Aromatic C=C	1446, 1490, 1508	1411, 1446, 1475	1431, 1473, 1517	1433, 1443, 1490
-C=S	1062	1060	-	-
-S-H	2555	2557	-	-
-C-H bending	754	759	764	758
=C-H bending	918	921	920	916
Ar-H bending	690	692	688	686
C-H stretching	3018	3053	3022	3034
Ar-H stretching	3097	3169	3080	3103
O-H stretching	3157	3257	3174	3246
N-H stretching	3244	3385	-	-
-OC-H stretching	2863	-	2848	-
V=O	-	-	972	975
V-S	-	-	464	462
V-N	-	-	511	509

the complexes ML_1 and ML_2 to 1627 cm^{-1} and 1624 cm^{-1} respectively, which is due to the involvement of the nitrogen atom of the amine groups in the coordination during complexes formation [18]. The weak stretching bands of the ligands, L_1, and L_2, were observed at 2555 cm^{-1} and 2557 cm^{-1} respectively due to ν(S−H) group disappearing in both the vanadium complexes confirming the participation of sulfur atom in complexation by deprotonation. It is clearly observed that these two weak bands due to the thiol group (−SH) and other two bands due to the thione group (C=S) at 1062 and 1060 cm^{-1} for respective ligands, seen in IR spectra of both the ligands illustrate the thione-thiol tautomerism of the Schiff bases [5, 15]. The weak and broad band observed at ~(3387−3236) cm^{-1} range could be assigned to the stretching vibrations of the O−H group. The appearance of the stretching band in the ligands at 3270-3394 cm^{-1} due to ν(N−H) stretching and disappearance in both the synthesized complexes is a good signal for the involvement of the sulfur in the coordination by the metals through the deprotonation of thiol form [25].

The stretching vibration bands that appeared at 464 cm^{-1} and 511 cm^{-1} could be contributed to the ν(V−S) and ν(V−N) bonds of the ML_1 complex, respectively. Similarly, these bands in ML_2 complexes are seen at 462 cm^{-1} and 509 cm^{-1} respectively [10]. This confirms that the vanadium atom in the final product is coordinated through the sulfur and nitrogen atoms. The stretching bands at 972 cm^{-1} and 975 cm^{-1} for ML_1 and ML_2 complexes contributed to the characteristic bands of ν(V=O), and are in agreement with other similar studies [6]. The weak band frequency of ν(C-OH) is observed between 1266-1305 cm^{-1} for the complexes and indicates the presence of free hydroxyl groups in the complexes [25].

3.2.2 Electronic spectra

The UV-visible spectral graphs of the complexes measured in DMSO solution from 200 to 800 nm range at room temperature are shown in **Fig. 3**. For both the complexes, the intense absorption band observed at 289 nm and 303 nm could be ascribed to n–π* transitions of the phenolic group, triazole ring, and azomethine groups. In the case of the electronic spectrum of ML_1 complex, the band at 335 nm is assigned to π–π* transitions of aromatic and triazole rings whereas the band due to π–π* transitions in these groups in ML_2 complex is detected at 320 nm. An intense band at 383 nm (ML_1) and at 389 nm (ML_2), are the characteristics of ligand to metal charge-transfer (LMCT) transition which is attributed to a charge-transfer between *p*π-orbital of the ligand and *d*π-orbital of vanadium metal [3]. The weak signals (459 nm and 467 nm) in the visible region is due to *d*-*d* transition in metal [5]. These four types of observed bands appear in the UV-Vis spectra of both complexes suggesting a square pyramidal geometry for VO(IV) complexes [6].

3.2.4 EPR spectra

The EPR spectra of 51V (nuclear spin I = 7/2) have the characteristic feature of possessing eight hyperfine lines with a variation in line width. Most of the vanadyl complexes have square pyramidal geometry and display lower symmetry than tetrahedral and octahedral complexes. This results in that the hyperfine splitting of the spectral line not being resolved properly in the complexes. This is due to higher nuclear moment and spin causing a broadening because of the longer relaxation time [11]. The X-band EPR spectra of oxovanadium(IV) complexes recorded at room temperature display a typical eight-line pattern of vanadium as shown in **Fig. 4** indicating the square pyramidal geometries of the tiny crystals of the synthesized complexes. The *g*-values for the complexes were determined from the spectra and was found to be *ca*. 1.98, which is very near to the free electron value of 2.00 confirming the d^1 state of vanadium in the complexes for its +4 oxidation number [3]. The *g*-values and the spectra are typical of the data reported for square pyramidal oxovanadium(IV) complexes with an unpaired *d*-electron [15]. The EPR data justifies the structure and geometry of the synthesized oxovanadium(IV) complexes due to its close agreement with the structural identity revealed from other spectral and computational results [11, 26].

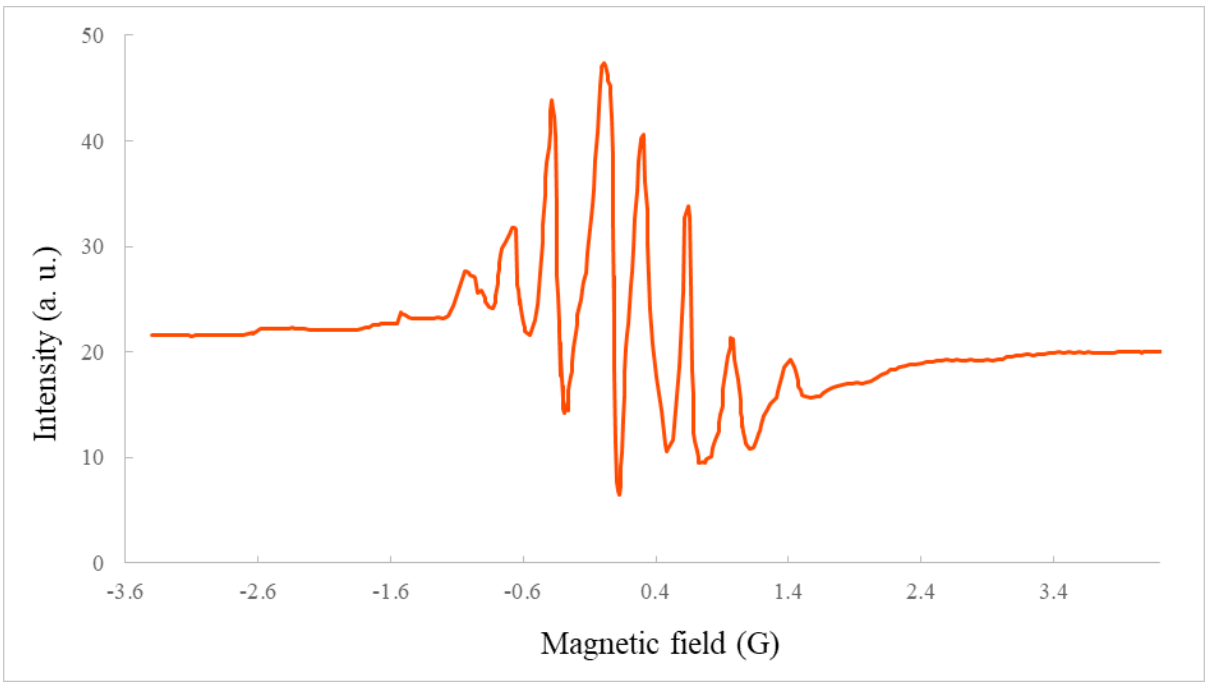

Fig. 3: *UV-Vis Spectra of the synthesized oxovanadium(IV) complexes, ML_1 and ML_2.*

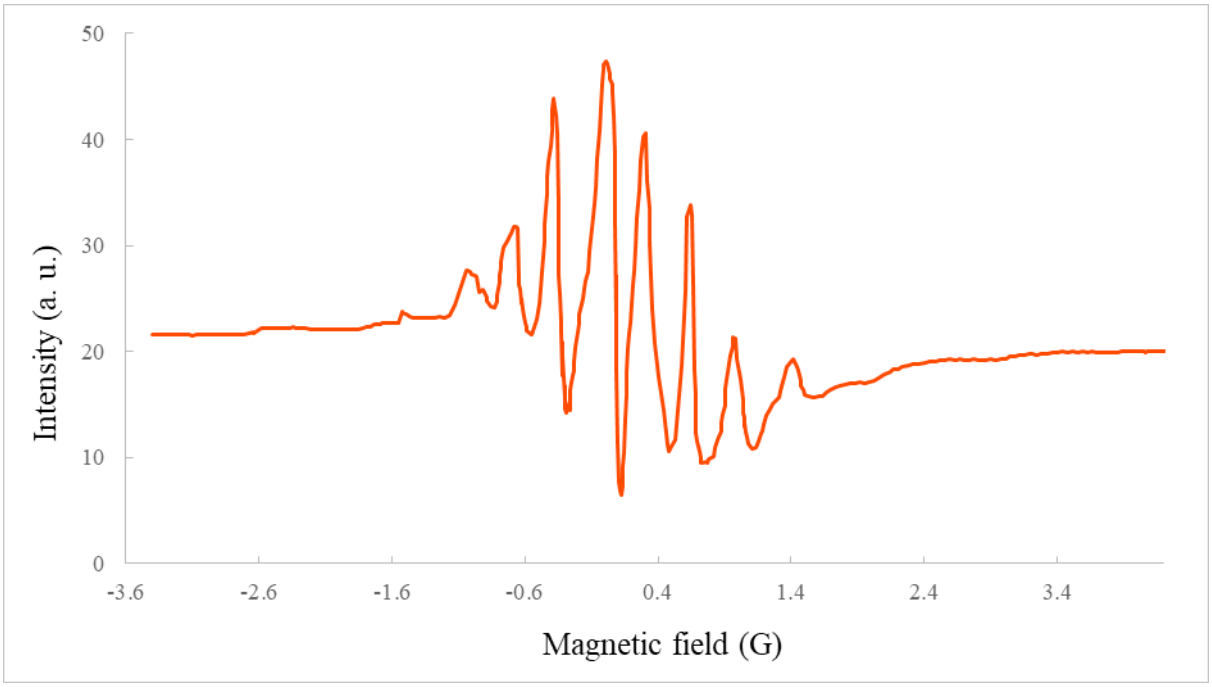

Fig. 4: *EPR spectra of one representative complex, ML_1 at room temperature.*

The structural models of the Schiff base ligands and their oxovanadium(IV) complexes are proposed as shown in **Fig. 5** with the help of elemental analysis and spectroscopic results. Based on the spectral analysis, the complexes possess a square pyramidal geometry as mentioned before with vanadium atom lying near the molecular center.

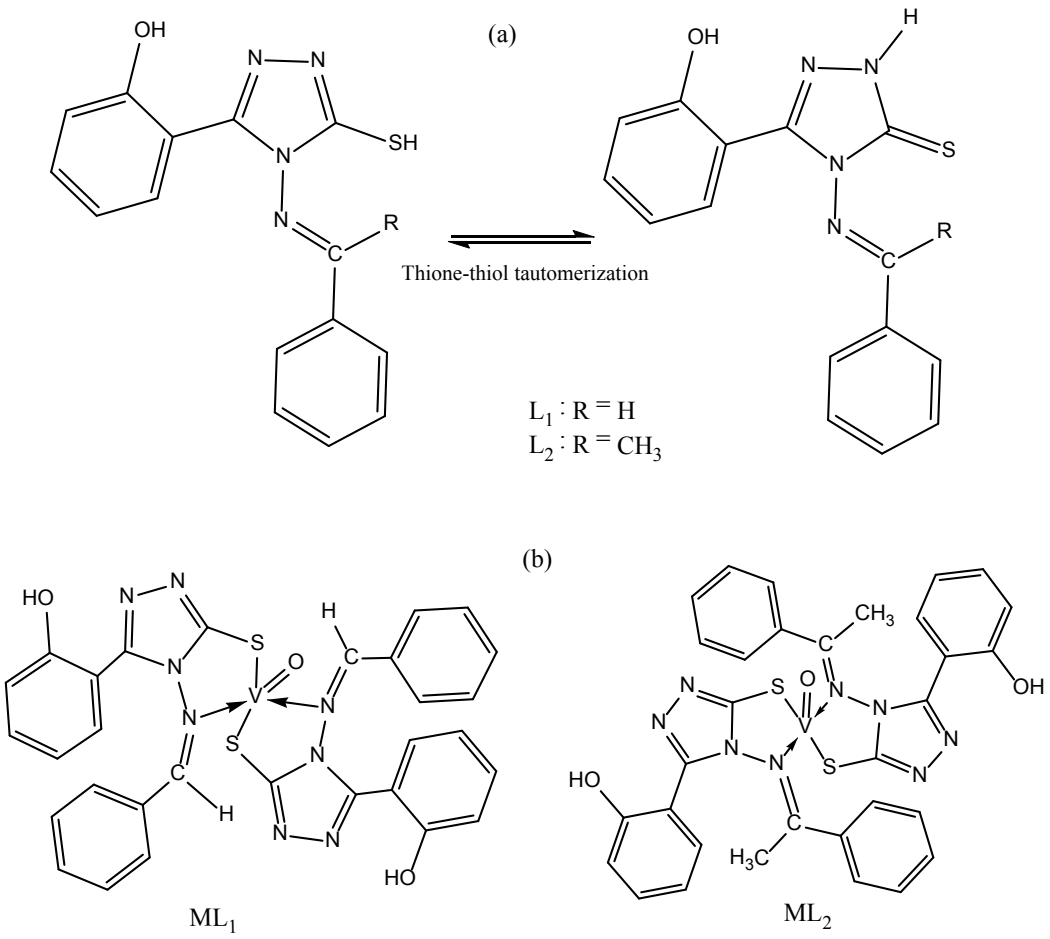

Fig. 5: *Proposed 2D structures of (a) tautomeric forms of Schiff bases and (b) oxovanadium(IV) complexes.*

3.3 XRD patterns analysis

Powder X-ray diffraction patterns of the oxovanadium(IV) complexes were obtained, to determine the crystalline structure of the complexes, and the observed pattern for a representative complex ML_1 is shown in **Fig. 6**. The crystallite size of both the complexes were calculated by using the Debye-Scherer formula. Here, FWHM was calculated by fitting the data using GSAS-II program [27]. The FWHM values of the most intense peaks of ML1 and ML_2 complexes were found to be 0.55° and 0.52° at the peak position of 2θ values 30.68° and 28.57° respectively. The crystallite size was found to be 15.64 nm and 16.46 nm for the two oxovanadium(IV) complexes, ML_1 and ML_2 respectively [15]. From the XRD data containing distinct peaks, it can be inferred that both the synthesized oxovanadium(IV) complexes of Schiff base ligands possess long range periodicity due to nano-crystalline morphology.

3.4 Conductance and cyclic voltammetry (CV) analysis

The molar conductance and the specific conductance of the solutions of both the complexes were measured to analyze their electrical behavior. It was found that they possess low conductance revealing their non-electrolytic nature [25]. The complexes ML_1 and ML_2 have molar conductance of 18.9 × 10^{-3} Sm^2mol^{-1} and 19.6 × 10-3Sm^2mol^{-1} respectively at a cell constant of 1.000 at room temperature whereas the specific conductance were 18.8 and 19.6 Siemens per meter (S/m).

The cyclic voltammograms of the millimolar solution of the complexes in DMSO containing 0.1M solution of tetrabutylammonium bromide as supporting electrolyte were recorded at a scan rate of 100 mV/s and a representative graph of ML1 complex is presented in **Fig. 7**. The cyclic voltammograms of the complexes show that the peak potential (ΔE_p) values lie in the range of 67±1 mV and the peak current ratio (I_a/I_c) in the 1.06±0.04 range (approximately 1) revealing one electron redox system of vanadium. The cyclic voltammograms for the complexes display the peak-to-peak separation, ΔE_p to be ~59 mV and 30 mV for a one-electron and two-electron processes respectively in an ideal reversible scenario [6, 12]. But in this study for both ML_1 and ML_2 complexes, the peak-to-peak separation is slightly larger, and the peak current ratio is nearly the same as in the one-electron ideal reversible process. Thus, it can be inferred that the electron transfer process in the redox system for these complexes is one-electron reduction and is quasi-reversible [28]. The peak current ratio was slightly larger than one and the peak current increased with the intensification of the scan rates

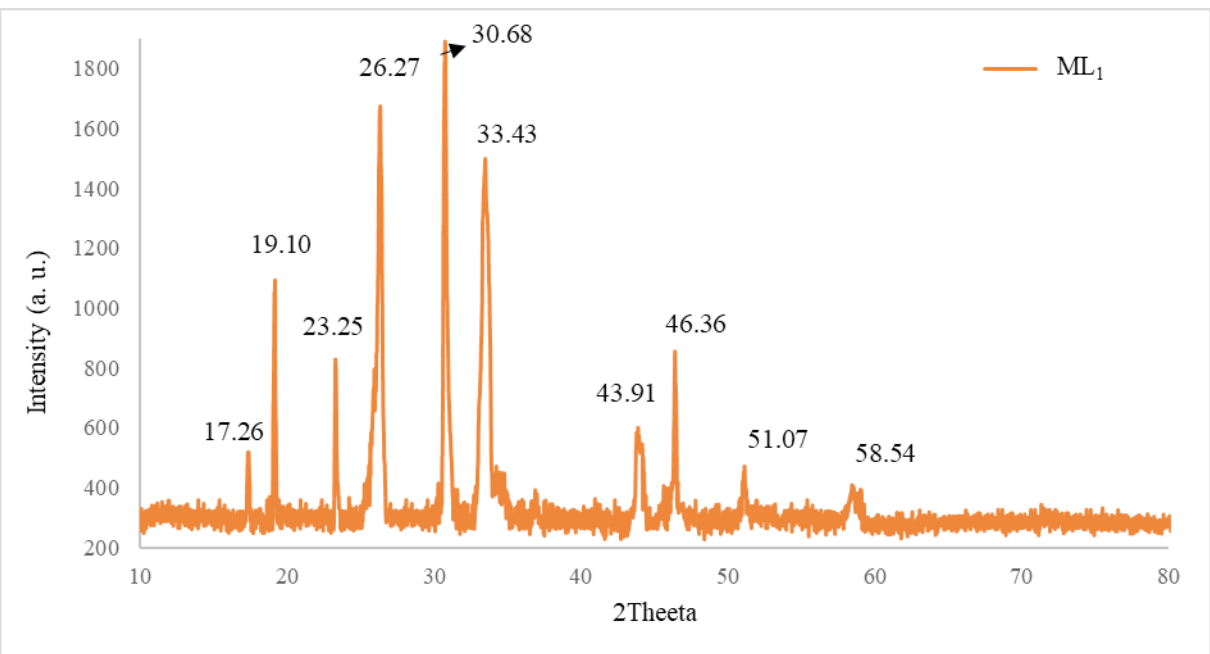

Fig. 6. Powder XRD patterns of a oxovanadium(IV) complexes ML_1.

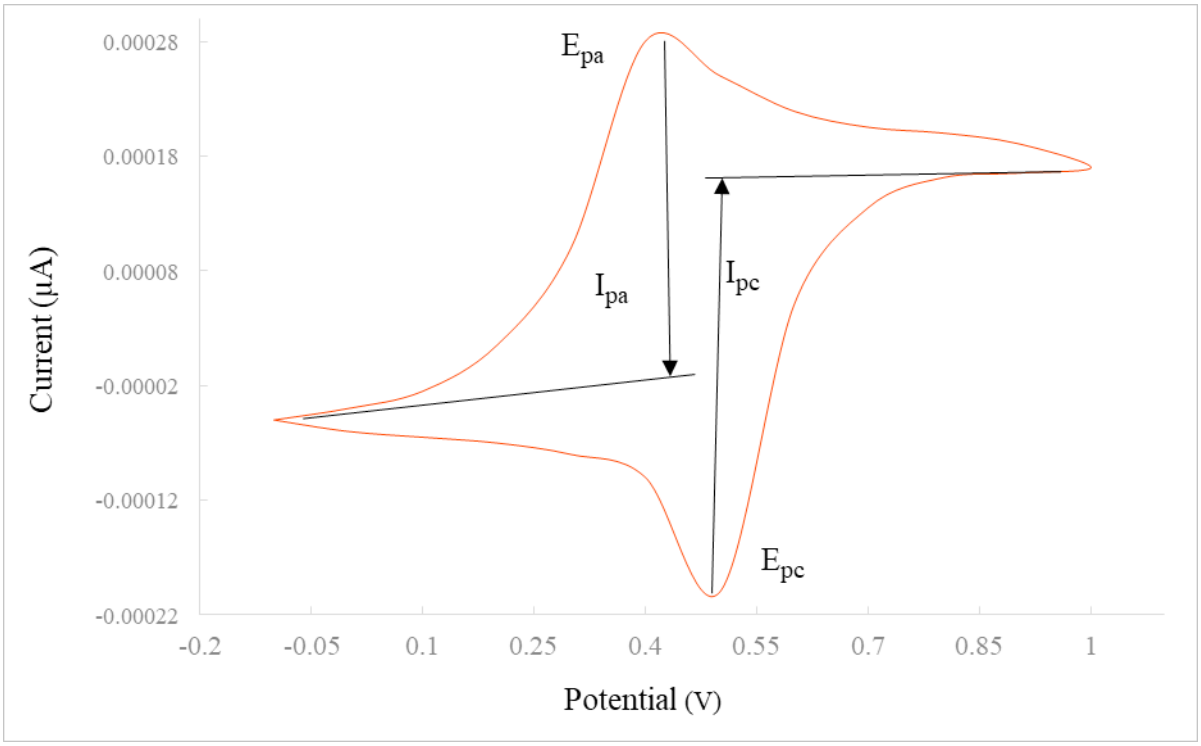

Fig. 7: *Cyclic voltammogram of ML_1 complex in DMSO at a scan rate of 100 mVs^{-1}.*

but the sharp increase in the anodic current was not observed which suggests the electrochemically stable nature of the complexes and the diffusion-controlled electrode process[6].

3.5 Computational simulations

3.5.1 Geometry optimization

The proposed structural models from the spectroscopic analysis (IR, UV-Vis, and EPR) were considered for the initial coordinates of atoms to formulate an initial structure for computational calculations. It was used in optimization of the molecular geometries in the gas phase using quantum mechanical calculation in the framework of DFT method. The final geometries were obtained with sequential optimization by tightening the criteria for optimization in every major step until the minimum energy structures were verified [3]. The structure of the ligands L1 and L2 were optimized to investigate the geometric and electronic features and to analyze their reactivity and chelating property. The ligand molecules have two head-on facing donating groups, one thiol, and one imine in the molecule (**Fig. 8**) with a dihedral angle of 13.9° (distance = 3.580 Å) and 8.3° (distance = 3.573 Å) respectively for $L_1$and L_2. This type of orientation of these donating groups supports the square pyramidal geometry of the complexes [6]. On the comparison between the free ligand and the formed complexes, slight elongation of the C=N bond of the imine group was observed in the metal coordination for ML_1 and ML_2 complexes, whereas the C-S bond of the thiol group was compressed a little upon coordination in both the complexes. Among the two bond angles between these groups, S-C8-N3, and C8-N3-N4 (**Fig. 8**), the first one showed a large decrease and the second one showed a slight change after complexation.

Some selected bond lengths and bond angles near the central vanadium atom in complexes are listed in **Table 3**. The angles indicated that the complexes adopted a distorted square pyramidal geometry.The optimized geometries of the studied molecules and the calculated parameters match well with other similar type of studies [7, 20, 28], and with the molecular structures deduced from the experimental techniques inferring a good validation of the theoretical results.

3.5.2 Reaction enthalpies

The optimization of the geometries of all ligands and complexes were carried out to obtain the total converged minimum energies of all isolated reactants and products (gas phases) and with the help of these

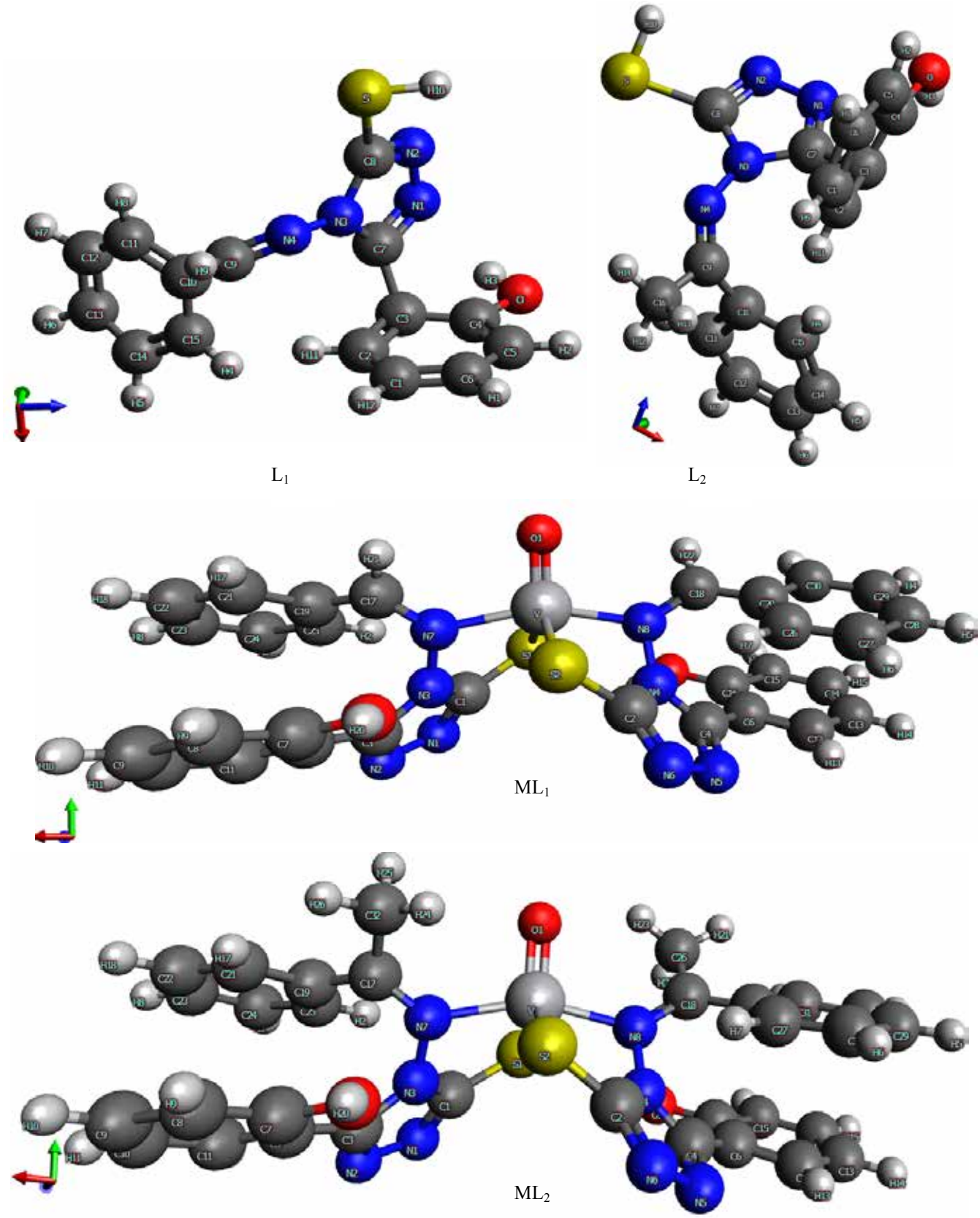

Fig. 8: *Optimized geometries of the studied molecules ML_1 and ML_2 (Carbon in dark gray, nitrogen in blue, oxygen in red, sulfur in golden yellow, vanadium in light gray (big sphere), and hydrogen in light gray (small sphere).*

Table 3: *Selectedbond lengthsandbond anglesofminimumenergystructuresofthecomplexes*

Bonds	Bond Lengths(Å)		Bonds	Bond Angles(°)	
	ML_1	ML_2		ML_1	ML_2
V=O1	1.603	1.606	S2-V-O1	116.1	113.9
V-N7	2.115	2.120	S1-V-O1	116.9	114.3
V-N8	2.112	2.110	N7-V-O1	100.7	101.5
V-S1	2.425	2.420	N8-V-O1	101.4	102.5
V-S2	2.412	2.417	S2-C2-N4	117.9	118.0
N4-N8	1.427	1.425	N3-C1-S1	118.0	118.2
N3-N7	1.423	1.424	C17-N7-V	133.3	132.0
C1-S1	1.752	1.751	C18-N8-V	134.6	134.6
C2-S2	1.748	1.747	N8-V-S1	87.3	86.8
N8-C18	1.315	1.321	N7-V-S2	88.4	88.1
N7-C17	1.315	1.318	N7-V-S1	82.3	82.7
N3-C1	1.405	1.402	N8-V-S2	82.9	82.8

values heat of reactions were calculated. The total energies (eV) of the molecules $VOSO_4$, H_2SO_4, L_1, ML_1, L_2, and ML_2 were found to be -4401.114, -2051.324, -4302.355, -10958.844, -4489.079, and -11334.034 respectively. The $\Delta H_{reaction}$ for the formation of complexes ML_1 and ML_2 were -4306.699 eV and -4495.165 eV respectively, calculated using the computed energies of the reactants and products of the reactions mentioned as in synthesis of oxovanadium(IV) complexes section. The total energies for the formation of both the complexes were negative i.e., total energy of products was less than that of the reactants in both the cases. This indicates that the metal complexes are stable, the reaction is energetically favorable, and the formation of complexes is spontaneous in nature [7].

3.5.3 FMOs

The highest occupied molecular orbital (HOMO) and lowest unoccupied molecular orbital (LUMO) are analyzed to determine the electronic involvement, chemical stability, and reactivity of the studied molecules. The HOMO characterizes the ability to donate an electron by the molecule and the LUMO represent the capability to accept an electron. Other different properties of the molecules like kinetic stability, chemical reactivity, polarizability, hardness, etc. are functions of HOMO and LUMO energy gap [7, 8] and were determined using previously reported equations [7]. These properties for different chemical species are organized in **Table 4**. All the calculated molecular orbitals (HOMO-1, HOMO, LUMO, LUMO+1) of the proposed models of different compounds are displayed in **Fig. 9**, **Fig. 10**, **Fig. 11**, and **Fig. 12** respectively.

Pictographic representation of the FMOs of all the ligands (L_1 and L_2) and complexes (ML_1 and ML_2) shows that the HOMOs of the molecules are mainly concentrated on the thiol group and triazole ring, whereas the LUMOs are mainly localized on the phenol ring and azomethine group. This suggests that thiol group of the ligand is involved in electron donation during complexation and azomethine group is involved in charge acquisition in back donation from the vanadium atom [29]. This type of mechanism is also supported by Mulliken and Hirshfeld charge analysis discussed later. The FMO results show that for both ML_1 and ML_2 complexes, the HOMO-LUMO gap (ΔE) is found to be reduced by nearly 1 eV than that of their corresponding ligands. The $\pi \rightarrow \pi^*$ electron transition between HOMO and LUMO and the charge transfer between ligands and metal are thus highly probable. This assertion was also supported by experimental electronic spectra for both the complexes where intense peaks due to these transitions are distinctly observed. Similar results have been reported in other similar studies [3, 6, 7].

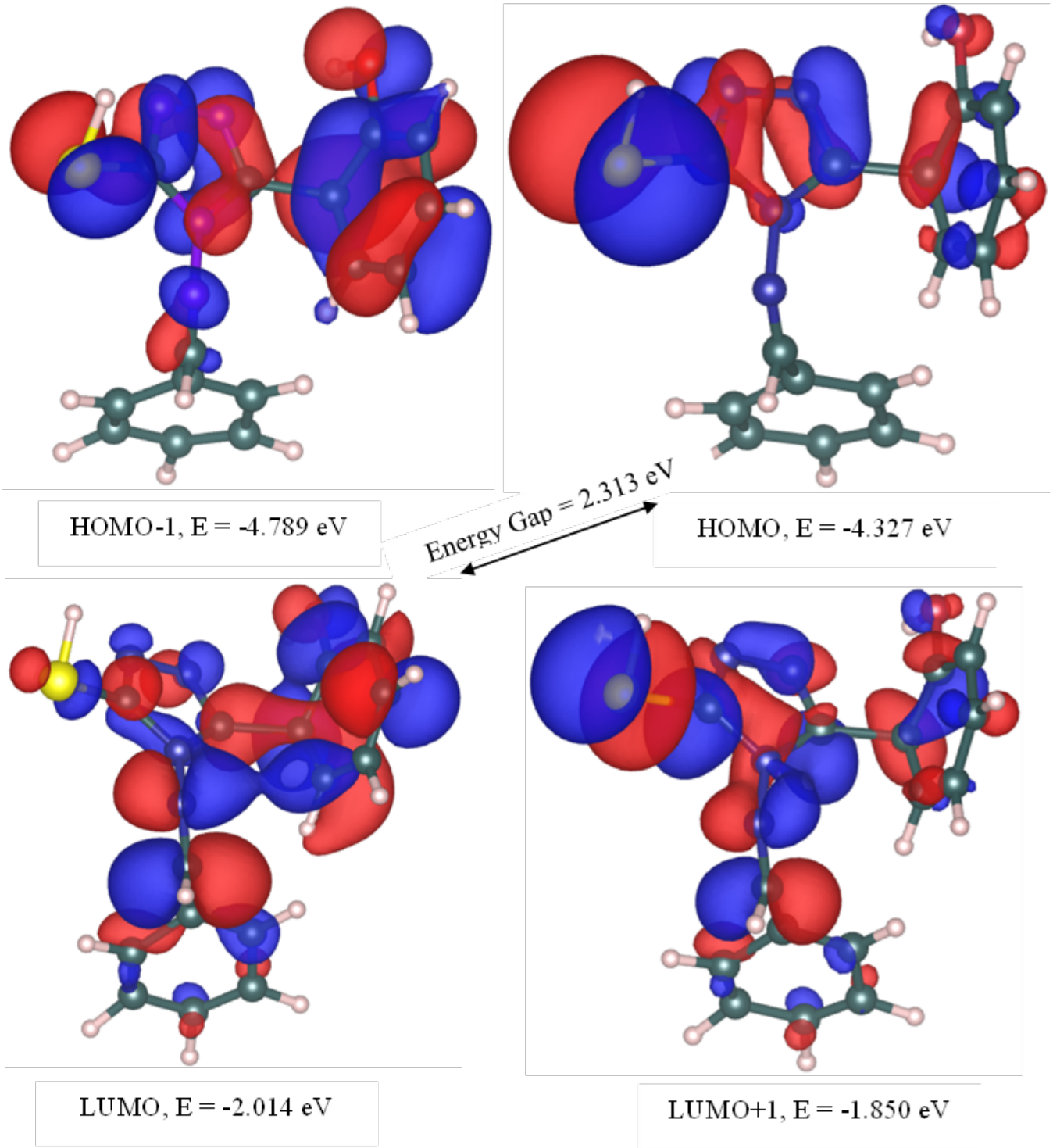

Fig. 9:*FMOs of ligand* L_1.

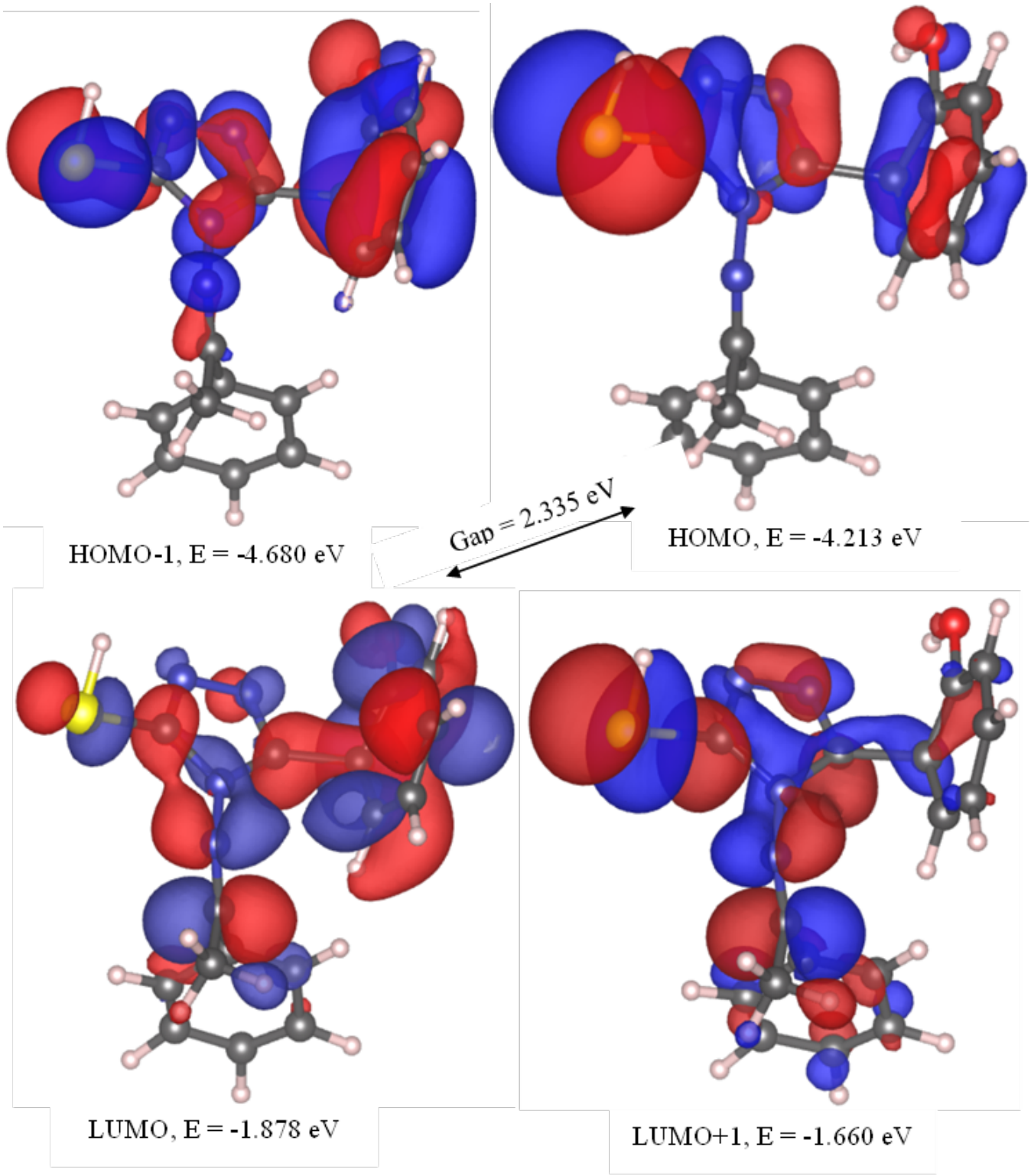

Fig. 10:*FMOs of ligand* L_2.

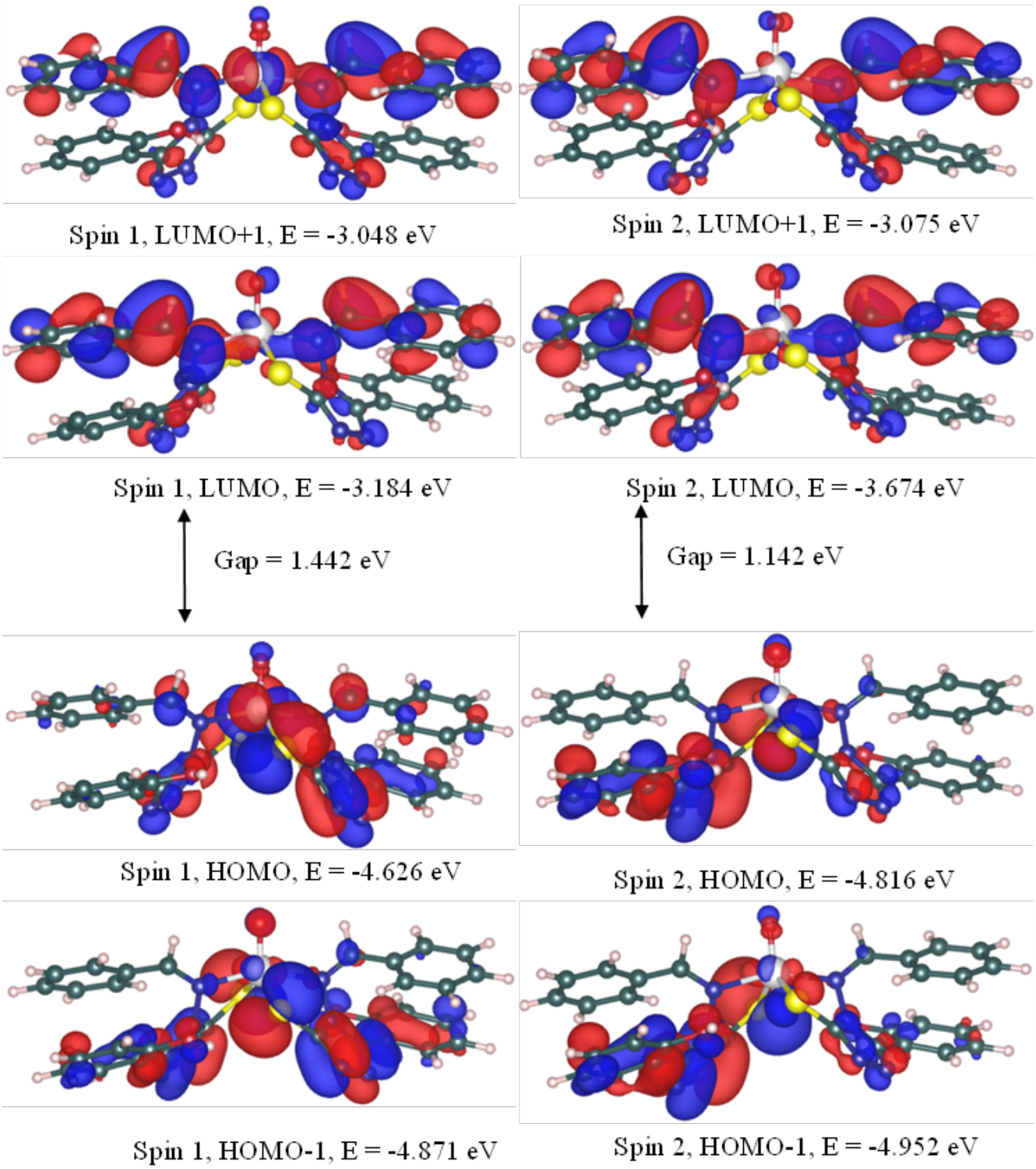

Fig. 11: *FMOs of ligand* ML_1.

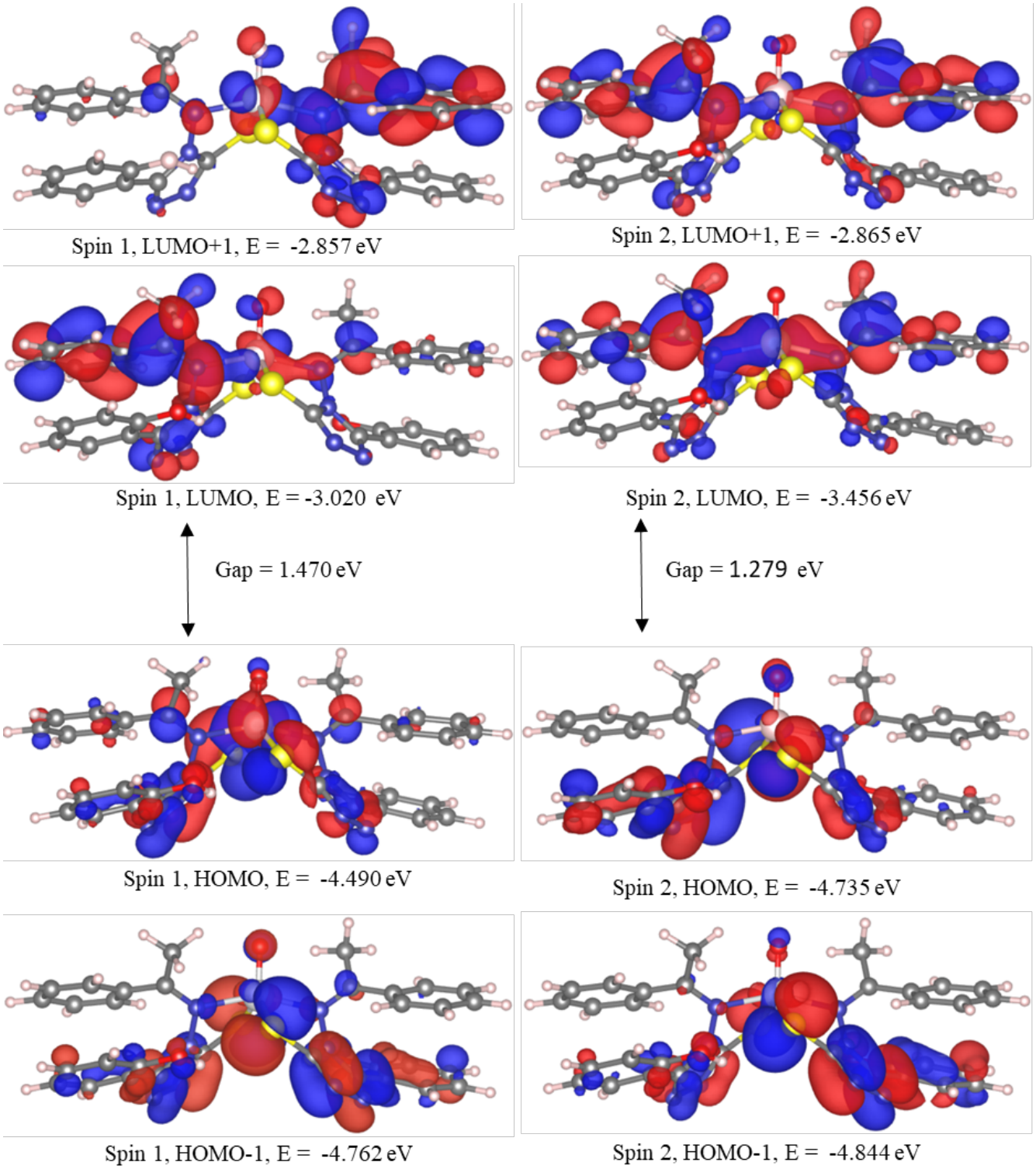

Fig. 12: *FMOs of the complex ML_2.*

Table 4: *HOMO-LUMO gap (ΔE) ionization energies (IE), electron affinities (EA), hardness, chemical potential, and electrophilicity of ligands and their complexes in gas phase*

Compounds		ΔE, (eV)	EA ($-E_{LUMO}$)	IE ($-E_{HOMO}$)	Chemical potential (μ)	Hardness (η)	Electrophilicity (ω)
L_1		2.313	2.014	4.327	-3.171	1.157	4.347
L_2		2.335	1.878	4.213	-3.046	1.168	3.973
ML_1	Spin1	1.442	3.184	4.626	-3.905	0.721	10.575
	Spin 2	1.142	3.674	4.816	-4.245	0.571	15.779
ML_2	Spin 1	1.470	3.02	4.49	-3.755	0.735	9.592
	Spin 2	1.279	3.456	4.735	-4.096	0.640	13.117

The small HOMO-LUMO energy gap in these compounds predict high chemical reactivity, enhanced softness, and reduced hardness (Table 4) of complexes than that of ligands. The comparison between two complexes disclosed that the ML_1 complex possess better reactivity, lesser stability, and superior hardness than ML_2 complex because of slightly lower orbital gap (considering the spin 1 state) [8]. Chemical potential is related to the electron donating property of compounds and electrophilicity is related to the electron accepting properties [3]. Thus, with the help of the chemical potential and electrophilicity values, it can be inferred that ML_1 complex is more electropositive and more reactive than the ML_2 complex.

3.5.4 Atomic charges and spins

The atomic charges and spins were determined from Mulliken and Hirshfeld population analysis of the complexes and is tabulated in **Table 5**. It can help in understanding the electron distribution throughout the molecules, geometries, polarizabilities, and the bonding nature [7, 26]. In both the cases it can be seen that the charge carried by vanadium tends to be low i.e., towards more negative value which infer transfer of electron density from ligands during the complex formation. The negative charge is also distributed over nitrogen and oxygen atoms which may be due to back donation of electrons from vanadium metal [7, 26]. Vanadium is a tetravalent electropositive atom but the net charges on it as shown by Mulliken formulation is found to be very small (positive value) and negative values are calculated by Hirshfeld formulation. This can be explained by considering the ligand to metal charge transfer mechanism whereby the charge is transferred from $p\pi$ to $d\pi$ orbitals [29] which is also supported by experimental findings and HOMO-LUMO studies of these complexes. The Mulliken and Hirshfeld spin analysis in both the complexes indicate that the spin of the molecule is mainly concentrated on vanadium atom and slightly distributed on other atoms which are directly attached to it. This infers towards the delocalization of the unpaired electron present in the *d*-orbital of the complexes [26]. Due to this type of electron delocalization and the charge transfer mechanism, the HOMOs of the complexes are concentrated in the coordination sphere around the vanadium and can be attributed to the origin of various interesting capabilities as discussed earlier.

3.5.5 Calculation of EPR g-value from the proposed models

The EPR *g*-value is an important parameter to analyze the paramagnetic compounds in terms of the presence of the metallic center with unpaired electron. It determines the nature of paramagnetic complexes and the interactions of unpaired electron spins with the nucleus can be analyzed. The DFT calculations on the models of the complexes ML_1 and ML_2 yielded the *g*-values to be 1.987 each [22, 30]. The obtained *g*-values for both the complexes are in close agreement with the *g*-values determined from the experiments, thus showing a reasonable validation of the proposed models containing proper bonding with the actual molecular structures of the complexes.

Table 5: *The calculated atomic charges and spins from optimized structures of the studied complexes*

Atoms	MullikenAnalysis				HirshfeldAnalysis			
	ML_1		ML_2		ML_1		ML_2	
	Net Charge	Spin Moment	Net Charge	Spin Moment	Net Charge	Spin Moment	Net Charge	Spin Moment
V	0.247	0.967	0.221	0.991	-1.333	0.902	-1.411	0.924
O1	-0.321	-0.109	-0.329	-0.109	0.172	-0.087	0.141	-0.088
S1	0.020	-0.010	0.023	-0.012	-0.116	0.002	-0.122	0.001
S2	0.040	-0.003	0.031	-0.005	-0.063	0.009	-0.085	0.008
C1	-0.004	0.002	-0.002	0.004	0.307	0.002	0.306	0.003
C2	-0.004	0.000	-0.001	0.001	0.308	0.001	0.309	0.002
N1	-0.213	-0.003	-0.216	0.004	-0.259	0.005	-0.261	0.004
N2	-0.163	-0.003	-0.167	0.000	-0.264	-0.001	-0.266	0.000
C3	0.113	0.004	0.113	0.002	0.224	0.003	0.222	0.002
N3	0.007	0.001	0.000	0.002	-0.077	0.000	-0.079	0.001
N4	-0.022	0.002	-0.027	0.003	-0.099	0.001	-0.099	0.003
C4	0.101	0.006	0.101	0.004	0.203	0.004	0.200	0.003
N5	-0.164	-0.004	-0.166	-0.002	-0.262	-0.002	-0.264	-0.001
N6	-0.213	0.009	-0.217	0.008	-0.260	0.008	-0.262	0.007
N7	-0.140	-0.048	-0.142	-0.043	0.147	-0.025	0.131	-0.022
N8	-0.147	-0.048	-0.151	-0.047	0.131	-0.025	0.113	-0.024
C5	-0.036	0.000	-0.036	0.000	0.010	0.000	0.011	0.000
C6	-0.041	-0.001	-0.040	-0.001	-0.006	0.000	-0.004	0.000
O2	-0.202	0.001	-0.204	0.001	-0.681	0.001	-0.695	0.001
O3	-0.198	0.001	-0.197	0.001	-0.706	0.001	-0.708	0.001

4. Conclusions

Two new oxovanadium(IV) complexes of triazole ring containing Schiff base ligands, 2-(4-(benzylidene amino)-5-mercapto-4H-1,2,4-triazol-3-yl)phenol and 2-(5-mercapto-4-((1-phenylethylidene)amino)-4H-1,2,4-triazol-3-yl)phenol were synthesized and characterized by various spectral and physicochemical techniques. The results obtained from different characterization techniques suggested square pyramidal geometries and established 2:1 molar ratio of ligand and VO2+ unit in the complexes. These findings were further supported by DFT results and revealed that the complexes were comparatively more reactive with augmented softness hinting towards enhanced biological activity. This work shows that computational method could be used as a supplementary and complementary tool in material characterization as a regular and user-friendly tool.

Acknowledgements

The authors are thankful to Central Department of Chemistry, Tribhuvan University, Kirtipur, Kathmandu and Nepal Academy of Science and Technology (NAST), Khumaltar, Lalitpur for various characterization related supports.

Declaration of competing interest

The authors declare that they have no any conflict of interest regarding the submission of this work.

References

1. J. Palion-Gazda, A. Luz, L. R. Raposo, K. Choroba, J. E. Nycz, A. Bieńko, A. Lewińska, K. Erfurt, P. V. Baptista, B. Machura, A. R. Fernandes, L. S. Shul'pina, N. S. Ikonnikov and G. B. Shul'pin, Vanadium(IV) complexes with methyl-substituted 8-hydroxyquinolines: catalytic potential in the oxidation of hydrocarbons and alcohols with peroxides and biological activity, *Molecules*, 2021, **26**(21), 6364. (DOI: 10.3390/molecules26216364).
2. B. Sergi, I. Bulut, Y. Xia, Z. A. E. Waller, Y. Yildizhan, C. Acilan and R. M. Lord, Understanding the potential *in vitro* modes of action of bis (β-diketonato) oxovanadium (IV) complexes, *ChemMedChem*, 2021, **16**(15), 2402–2410. (DOI: 10.1002/cmdc.202100152).
3. A. S. Basaleh, F. Y. Alomari, A. A. Sharfalddin, N. S. Al-Radadi, D. Domyati and M. A. Hussien, Theoretical investigation by DFT and molecular docking of synthesized oxidovanadium (IV)-based imidazole drug complexes as promising anticancer agents, *Molecules*, 2022, **27**(9), 2796. (DOI: 10.3390/molecules27092796).
4. F. D. Kalındemirtaş, B. Kaya, E. Sert, O. Şahin, S. E. Kuruca and B. Ülküseven, New oxovanadium(IV) complexes overcame drug resistance and increased *in vitro* cytotoxicity by an apoptotic pathway in breast cancer cells, *Chemico-Biological Interactions*, 2022, **363**, 109997. (DOI: 10.1016/j.cbi.2022.109997).
5. D. Domyati, S. A. Zabin, A. A. Elhenawy and M. Abdelbaset, Preparation, antimicrobial activity and docking study of vanadium mixed ligand complexes containing 4-amino-5-hydrazinyl-4H-1,2,4-triazole-3-thiol and aminophenol derivatives, *Processes*, 2021, **9**(6), 1008. (DOI: 10.3390/pr9061008).
6. D. Aggoun, Z. Messasma, B. Bouzerafa, R. Berenguer, E. Morallon, Y. Ouennoughi and A. Ourari, Synthesis, characterization and DFT investigation of new metal complexes of Ni(II), Mn(II) and VO(IV) containing N,O-donor Schiff base ligand, *Journal of Molecular Structure*, 2021, **1231**, 129923. (DOI: 10.1016/j.molstruc.2021.129923).
7. S. A. Rupa, Md. R. Moni, Md. A. M. Patwary, Md. M. Mahmud, Md. A. Haque, J. Uddin and S. M. T. Abedin, Synthesis of novel tritopic hydrazone ligands: spectroscopy, biological activity, DFT, and molecular docking studies, *Molecules*, 2022, **27**(5), 1656. (DOI: 10.3390/molecules27051656).
8. R. Omidinia, S. Ali Beyramabadi, S. Allameh, A. Morsali and M. Pordel, Synthesis, characterization, DFT and antibacterial studies of a novel vitamin B6 Schiff base and its Cu(II) and Zn(II) complexes, *Journal of Molecular Structure*, 2022, **1248**, 131452. (DOI: 10.1016/j.molstruc.2021.131452).
9. P. K. Sahoo, R. Sharma and P. Pattanayak, Synthesis and evaluation of 4-amino-5-phenyl-4H-[1,2,4]-triazole-3-thiol derivatives as antimicrobial agents, *Medicinal Chemistry Research*, 2010, **19**(2), 127–135. (DOI: 10.1007/s00044-009-9178-8).
10. F. M. A. Altalbawy, G. G. Mohamed, M. Abou El-Ela Sayed and M. I. A. Mohamed, Synthesis, characterization, and biological activity of some transition metal complexes with Schiff base ligands derived from 4-amino-5-phenyl-4H-1,2,4-triazole-3-thiol and salicaldehyde, *Monatshefte für Chemie - Chemical Monthly*, 2012, **143**(1), 79–89. (DOI: 10.1007/s00706-011-0626-z).
11. M. L. Sharma, A. K. Srivastava, B. P. Sharma, B. P. Marasini, O. P. Pandey and S. K. Sengupta, Synthesis, physicochemical studies and biological applications of oxovanadium(IV) complexes with Schiff bases derived from 3-phenyl-4-amino-5-mercapto-1, 2, 4-triazoles and benzil, *International Journal of Advanced Research*, 2022, **10**(04), 841–854. (DOI: 10.21474/IJAR01/14621).
12. B. P. Sharma, S. K. Pandey, B. P. Marasini, S. Shrestha and M. L. Sharma, Oxovanadium(IV) complexes with triazole based Schiff base ligands: synthesis, characterization and antibacterial study, *Journal of Nepal Chemical Society*, 2021, **42**(1), 56–63. (DOI: 10.3126/jncs.v42i1.35332).

13. B. Kołodziej, M. Morawiak, W. Schilf and B. Kamieński, Structure investigations of Schiff bases derived from 3-amino-1H-1,2,4-triazole, *Journal of Molecular Structure*, 2019, **1184**, 207–218. (DOI: 10.1016/j.molstruc.2019.02.027).

14. M. L. Sharma, S. K. Sengupta and O. P. Pandey, Template synthesis, spectroscopic characterization and preliminary insulin-mimetic activity of oxovanadium(IV) complexes with N_2O_2 diazadioxa macrocycles, *Spectrochimica Acta Part A: Molecular and Biomolecular Spectroscopy*, 2012, **95**, 562–568. (DOI: 10.1016/j.saa.2012.04.050).

15. M. K. Sahani, S. K. Pandey, O. P. Pandey and S. K. Sengupta, A series of novel oxovanadium(IV) complexes: Synthesis, spectral characterization and antimicrobial study, *Journal of Molecular Structure*, 2014, **1074**, 401–407. (DOI: 10.1016/j.molstruc.2014.06.015).

16. E. J. F. Dickinson, J. G. Limon-Petersen, N. V. Rees and R. G. Compton, How much supporting electrolyte is required to make a cyclic voltammetry experiment quantitatively "diffusional"? A theoretical and experimental investigation, *The Journal of Physical Chemistry C*, 2009, **113**(25), 11157–11171. (DOI: 10.1021/jp901628h).

17. T. D. Kühne, M. Iannuzzi, M. Del Ben, V. V. Rybkin, P. Seewald, F. Stein, T. Laino, R. Z. Khaliullin, O. Schütt, F. Schiffmann, D. Golze, J. Wilhelm, S. Chulkov, M. H. Bani-Hashemian, V. Weber, U. Borštnik, M. Taillefumier, A. S. Jakobovits, A. Lazzaro, H. Pabst, T. Müller, R. Schade, M. Guidon, S. Andermatt, N. Holmberg, G. K. Schenter, A. Hehn, A. Bussy, F. Belleflamme, G. Tabacchi, A. Glöß, M. Lass, I. Bethune, C. J. Mundy, C. Plessl, M. Watkins, J. VandeVondele, M. Krack and J. Hutter, CP2K: An electronic structure and molecular dynamics software package - Quickstep: Efficient and accurate electronic structure calculations, *The Journal of Chemical Physics*, 2020, **152**(19), 194103. (DOI: 10.1063/5.0007045).

18. T. M. A. Al-Shboul, M. El-khateeb, Z. H. Obeidat, T. S. Ababneh, S. S. Al-Tarawneh, M. S. Al Zoubi, W. Alshaer, A. Abu Seni, T. Qasem, H. Moriyama, Y. Yoshida, H. Kitagawa and T. M. A. Jazzazi, Synthesis, characterization, computational and biological activity of some Schiff bases and their Fe, Cu and Zn complexes, *Inorganics*, 2022, **10**(8), 112. (DOI: 10.3390/inorganics10080112).

19. R. Haunschild, A. Barth and W. Marx, Evolution of DFT studies in view of a scientometric perspective, *Journal of Cheminformatics*, 2016, **8**(1), 52. (DOI: 10.1186/s13321-016-0166-y).

20. S. Akkoc, H. Karatas, M. T. Muhammed, Z. Kökbudak, A. Ceylan, F. Almalki, H. Laaroussi and T. Ben Hadda, Drug design of new therapeutic agents: molecular docking, molecular dynamics simulation, DFT and POM analyses of new Schiff base ligands and impact of substituents on bioactivity of their potential antifungal pharmacophore site, *Journal of Biomolecular Structure and Dynamics*, 2022, 1–14. (DOI: 10.1080/07391102.2022.2111360).

21. E. Aprà, E. J. Bylaska, W. A. de Jong, N. Govind, K. Kowalski, T. P. Straatsma, M. Valiev, H. J. J. van Dam, Y. Alexeev, J. Anchell, V. Anisimov, F. W. Aquino, R. Atta-Fynn, J. Autschbach, N. P. Bauman, J. C. Becca, D. E. Bernholdt, K. Bhaskaran-Nair, S. Bogatko, P. Borowski, J. Boschen, J. Brabec, A. Bruner, E. Cauët, Y. Chen, G. N. Chuev, C. J. Cramer, J. Daily, M. J. O. Deegan, T. H. Dunning, M. Dupuis, K. G. Dyall, G. I. Fann, S. A. Fischer, A. Fonari, H. Früchtl, L. Gagliardi, J. Garza, N. Gawande, S. Ghosh, K. Glaesemann, A. W. Götz, J. Hammond, V. Helms, E. D. Hermes, K. Hirao, S. Hirata, M. Jacquelin, L. Jensen, B. G. Johnson, H. Jónsson, R. A. Kendall, M. Klemm, R. Kobayashi, V. Konkov, S. Krishnamoorthy, M. Krishnan, Z. Lin, R. D. Lins, R. J. Littlefield, A. J. Logsdail, K. Lopata, W. Ma, A. V. Marenich, J. Martin del Campo, D. Mejia-Rodriguez, J. E. Moore, J. M. Mullin, T. Nakajima, D. R. Nascimento, J. A. Nichols, P. J. Nichols, J. Nieplocha, A. Otero-de-la-Roza, B. Palmer, A. Panyala, T. Pirojsirikul, B. Peng, R. Peverati, J. Pittner, L. Pollack, R. M. Richard, P. Sadayappan, G. C. Schatz, W. A. Shelton, D. W. Silverstein, D. M. A. Smith, T. A. Soares, D. Song, M. Swart, H. L. Taylor, G. S. Thomas, V. Tipparaju, D. G. Truhlar, K. Tsemekhman, T. Van Voorhis, Á. Vázquez-Mayagoitia, P. Verma, O. Villa, A. Vishnu, K. D. Vogiatzis, D. Wang, J. H. Weare, M. J. Williamson, T. L. Windus, K. Woliński, A. T. Wong, Q. Wu, C. Yang, Q. Yu, M. Zacharias, Z. Zhang, Y. Zhao and R. J.

Harrison, Nwchem: Past, present, and future, *The Journal of Chemical Physics*, 2020, **152**(18), 184102. (DOI: 10.1063/5.0004997).

22. G. Sciortino, G. Lubinu, J.-D. Maréchal and E. Garribba, DFT protocol for EPR prediction of paramagnetic Cu(II) complexes and application to protein binding sites, *Magnetochemistry*, 2018, **4**(4), 55. (DOI: 10.3390/magnetochemistry4040055).

23. M. D. Hanwell, D. E. Curtis, D. C. Lonie, T. Vandermeersch, E. Zurek and G. R. Hutchison, Avogadro: an advanced semantic chemical editor, visualization, and analysis platform, *Journal of Cheminformatics*, 2012, **4**(1), 17. (DOI: 10.1186/1758-2946-4-17).

24. K. Momma and F. Izumi, *VESTA 3* for three-dimensional visualization of crystal, volumetric and morphology data, *Journal of Applied Crystallography*, 2011, **44**(6), 1272–1276. (DOI: 10.1107/S0021889811038970).

25. T. Damena, D. Zeleke, T. Desalegn, T. B. Demissie and R. Eswaramoorthy, Synthesis, characterization, and biological activities of novel vanadium(IV) and cobalt(II) complexes, *ACS Omega*, 2022, **7**(5), 4389–4404. (DOI: 10.1021/acsomega.1c06205).

26. R. C. Maurya, A. K. Sharma, P. K. Vishwkarma, J. M. Mir, B. A. Malik and D. K. Rajak, Two novel sugar schiff base oxovanadium (IV) complexes: Their synthesis, characterization by combined DFT-experimental approach and thermal studies, *Journal of Ravishankar University PART-B*, 2015, **28**(1), 11–29.

27. B. H. Toby and R. B. Von Dreele, *GSAS-II*: the genesis of a modern open-source all purpose crystallography software package, *Journal of Applied Crystallography*, 2013, **46**(2), 544–549. (DOI: 10.1107/S0021889813003531).

28. A. Banerjee, M. Mohanty, S. Lima, R. Samanta, E. Garribba, T. Sasamori and R. Dinda, Synthesis, structure and characterization of new dithiocarbazate-based mixed ligand oxidovanadium(IV) complexes: DNA/HSA interaction, cytotoxic activity and DFT studies, *New Journal of Chemistry*, 2020, **44**(26), 10946–10963. (DOI: 10.1039/D0NJ01246G).

29. P. M. A. Machado, R. A. Allão Cassaro, V. M. de Assis, S. de P. Machado, A. Horn and E. R. Lachter, Synthesis, characterization and DFT studies of a new unsymmetrical dinuclear vanadium(IV) complex with a bipodal N2O-donor ligand, *Journal of Molecular Structure*, 2019, **1193**, 110–117. (DOI: 10.1016/j.molstruc.2019.04.098).

30. F. Aquino, B. Pritchard and J. Autschbach, Scalar relativistic computations and localized orbital analyses of nuclear hyperfine coupling and paramagnetic NMR chemical shifts, *Journal of Chemical Theory and Computation*, 2012, **8**(2), 598–609. (DOI: 10.1021/ct2008507).